# Structure (1.3 Å) and Charge States of a Ribonuclease A−Uridine Vanadate Complex: Implications for the Phosphate Ester Hydrolysis Mechanism

**Brian D. Wladkowski,[†] L. Anders Svensson,[‡] Lennart Sjolin,[§] Jane E. Ladner,[||] and Gary L. Gilliland*,[||]**

*Contribution from the Department of Chemistry, Western Maryland College, 2 College Hill, Westminster, Maryland 21157, Department of Molecular Biophysics, Chemical Center, Lund University, Box 124, S-221 00, Lund, Sweden, Department of Inorganic Chemistry, Chalmers University of Technology and The University of Goteborg, S-412 96 Goteborg, Sweden, and The Center for Advanced Research in Biotechnology of the University of Maryland Biotechnology Institute and National Institute of Standards and Technology, 9600 Gudelsky Drive, Rockville, Maryland 20850*

*Received July 9, 1997. Revised Manuscript Received November 19, 1997*

**Abstract:** A joint X-ray crystallographic (1.3 Å resolution) and ab initio quantum mechanical analysis of a uridine vanadate−ribonuclease A complex (UV−RNase A) is undertaken to probe specific aspects of the microscopic mechanism by which ribonuclease functions to catalyze the hydrolysis of its natural substrate, phosphate esters. Comparison of the structural features of the vanadate portion from the final X-ray refinement with the oxy-vanadate model compounds determined computationally provides direct evidence of the likely protonation state of the UV inhibitor bound in the active site. Specifically, the UV bound in the active site of UV−RNase A is found to be monoanionic, and the most likely source of this proton is from the active site residue His12. Together with the structural data, these results strongly suggest that even though His12 may act as the catalytic base in the first step of the mechanism, transphosphorylation, and the catalytic acid in the second step, hydrolysis, it must also play an additional, although perhaps secondary, role in stabilizing the pentacoordinate phosphorane structure through proton transfer. On the basis of its close proximity to critical vanadate oxygen in the UV, and data obtained from a previous computational study, Lys41 is likely to play a more intimate role in the catalytic mechanism than previously proposed, potentially acting as the catalytic base in certain cases. Two possible detailed microscopic mechanisms are presented.

## Introduction

Bovine pancreatic ribonuclease A (EC 3.1.27.5; RNase A), a protein composed of a single chain of 124 amino acid residues, efficiently catalyzes the hydrolysis of phosphate ester linkages in single-stranded RNA. RNase A has been the subject of numerous biochemical, biophysical, and structural studies aimed at resolving various issues surrounding its catalytic function and has emerged as a prototype model enzyme by which other systems are compared (for reviews, see Richards and Wyckoff,[1] Blackburn and Moore,[2] and Wlodawer[3]). Since the initial structure determination studies by Kartha et al.[4] and Avey et al.[5] in 1967, RNase A and its subtilisin cleaved form, RNase S, which was first isolated by Richards and Vithayathil[6] in 1959, have continued to be the subject of many crystallographic studies[7−14] using both X-ray and neutron diffraction techniques. The most recent studies have extended the structure determination to very high resolution (<1.5 Å), providing new details of the enzyme's atomic structure including its enzymatic functionality. Some of the structures determined at high resolution thus far include the enzyme with phosphate or sulfate bound in the active site and the unligated form. The structures of several ribonuclease complexes, including those containing inhibitors and nucleotide analogues, have also been determined,[15−17] leading to a further understanding of the structural features essential for substrate binding and enzyme

[†] Western Maryland College.
[‡] Lund University.
§Chalmers University of Technology and The University of Goteborg.
[||] The Center for Advanced Research in Biotechnology.

(1) Richards, F. M.; Wyckoff, H. W. In *The Enzymes*; Boyer, P. D., Ed; Academic Press: New York, 1971; Vol. 4.
(2) Blackburn, P.; Moore, S. In *The Enzymes*; Boyer, P. D., Ed; Academic Press: New York, 1982; Vol. 15.
(3) Wlodawer, A. In *Biological Macromolecules and Assemblies: Nucleic acids and interactive proteins*; Jurnak, F., McPherson, A., Eds.; John Wiley & Sons: New York, 1984; Vol. 2.
(4) Kartha, G.; Bello, J.; Harker, D. *Nature* **1967**, *213*, 862−865.
(5) Avey, H. P.; Boles, M. O.; Carlisle, C. H.; Evans, S. A.; Morris, S. J.; Palmer, R. A.; Woolhouse, B. A.; Shall, S. *Nature* **1967**, *213*, 557−562.
(6) Richards, F. M.; Vithayathil, P. J. *J. Biol. Chem.* **1959**, *234*, 1459−1465.
(7) Wyckoff, H. W.; Tsernoglou, D.; Hanson, A. W.; Knox, J. R.; Lee, B.; Richards, F. M. *J. Biol. Chem.* **1970**, *245*, 305−328.
(8) Wlodawer, A.; Bott, R.; Sjolin, L. *J. Biol. Chem.* **1982**, *257*, 1325−1332.
(9) Wlodawer, A.; Sjolin, L. *Biochemistry* **1983**, *22*, 2720−2728.
(10) Borkakoti, N.; Moss, D. S.; Stanford, M. J.; Palmer, R. *J. Crystallogr. Spectrosc. Res.* **1984**, *14*, 467−494.
(11) Campbell, R.; Petsko, G. A. *Biochemistry* **1987**, *26*, 8579−8584.
(12) Wlodawer, A.; Svensson, A. A.; Sjölin, L.; Gilliland, G. L. *Biochemistry* **1988**, *27*, 2705−27l7. Phosphate-free ribonuclease A was refined at 1.26 Å resolution.
(13) Svensson, L. A.; Sjolin, L.; Dill, J.; Gilliland, G. L. In *Structure, Mechanism and Function of Ribonucleases*; Cuchillo, C. M., de Llorens, R., Nogues, M. V., Pares, X., Eds.; IBF Publications Universitat Autonoma de Barecelona: Barcelona, 1991.
(14) Kim, E. E.; Varadarajan, R.; Wyckoff, H. W.; Richards, F. M. *Biochemistry* **1992**, *31*, 12304−12314.

S0002-7863(97)02296-8 CCC: $15.00 
Published on Web 05/27/1998

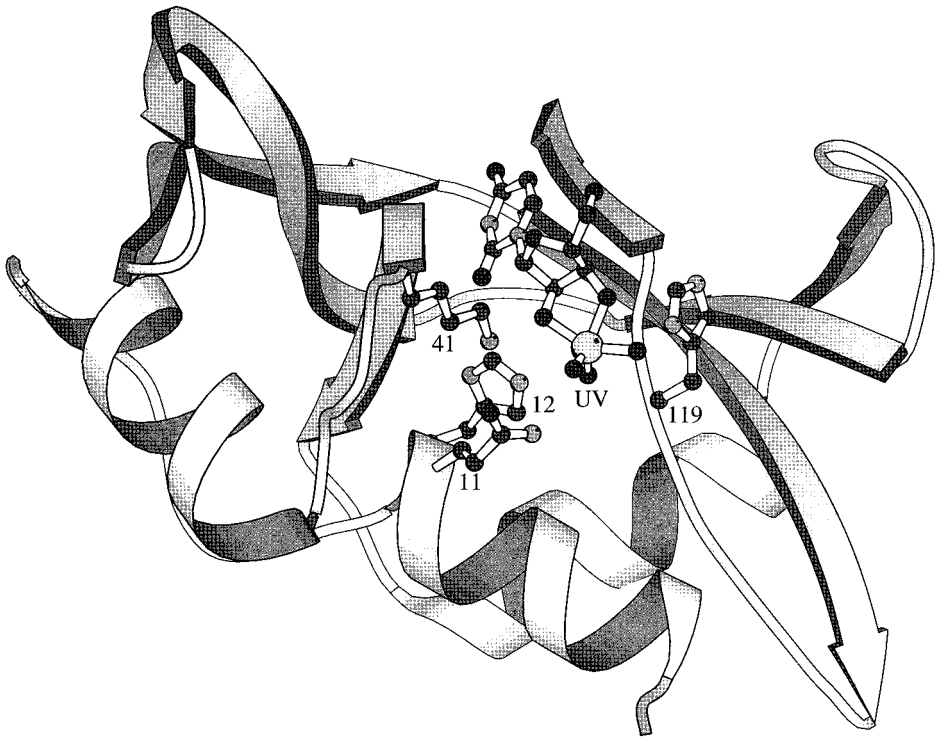


**Figure 1.** $C_\alpha$ backbone of 1RUV with the important active site side chains showing.

catalysis. In addition, structural investigations of semisynthetic variants of ribonuclease have been carried out to address specific questions concerning catalysis and how the change of a specific amino acid residue can influence the structure.[18−20] Collectively, the structural work on RNase A has provided valuable insight into many aspects of the function of this enzyme, including many qualitative features of the catalytic mechanism. Shown in Figure 1 is a three-dimensional ribbon representation of the $C_\alpha$ backbone of UV−RNase A complex with the UV (uridine vanadate) and important active site residues, Gln11, His12, Lys41, and His119, identified.

The generally accepted mechanism by which RNase A catalyzes phosphate ester hydrolysis is the two step general acid/general base mechanism shown in Figure 2. In the first step, the 3′−5′ phosphate linkage is cleaved via intramolecular transphosphorylation leading to a 2′−3′ cyclic phosphate intermediate. In the subsequent step, the cyclic phosphate is hydrolyzed by a water molecule within the active site to form a 3′ monophosphate ester as the final product. Both steps in the reaction are known to proceed by an in-line inversion displacement mechanism based on isotopic labeling experiments.[21,22] As seen in Figure 2, His12 and His119 are proposed as the critical catalytic residues in the enzyme active site. These two residues are thought to act as the general base and general acid, respectively, in the first step, reversing their roles in the second step of the reaction. Other residues within the active site, such as Lys41 and Asp121, are also catalytically important based on chemical modification and site-directed mutagenesis studies;[23−25] however, their specific role in the catalytic mechanism remains unclear. Of these important residues, the role of Lys41 has been the most highly debated. The position of Lys41 within the active site allows for direct contact with the substrate, and it has been argued[26] that this residue acts to stabilize anionic intermediates through electrostatic interactions; however, this has never been verified.

Despite the considerable progress made in characterizing the qualitative aspects of the RNase A catalytic mechanism, many questions regarding the microscopic details remain unresolved. Much of the controversy centers around the nature of the intermediate(s) that may exist along the reaction pathway and the details of the steps which form them, including catalytic proton transfer steps. As indicated in Figure 2, a pentacoordinate trigonal bipyramid (TBP) phosphorane is postulated to be an important structure along the reaction pathway, consistent with the "in-line" inversion displacement mechanism. The actual character of the TBP phosphorane structure, including its protonation state and whether it is a transition state or a true intermediate, has been an issue of considerable debate over the years. Naturally, the inability to directly probe such intermediates has been a serious obstacle to a more complete understanding of many enzymatic reaction mechanisms, including that of RNase A.

Lindquist and co-workers[27] proposed that a complex of uridine with certain oxy-vanadium compounds, which can

(15) Wodak, S. Y.; Liu, M. Y.; Wyckoff, H. W. *J. Mol. Biol.* **1977**, *116*, 855−875.
(16) Howlin, B.; Harris, G. W.; Moss, D. S.; Palmer, R. A. *J. Mol. Biol.* **1987**, *196*, 159−164.
(17) Zegers, I.; Maes, D.; Dao-Thi, M.-H.; Poortmans, F.; Palmer, R.; Wyns, L. *Protein Sci.* **1994**, *3*, 2322−2339.
(18) Taylor, H. C.; Kormoriya, A.; Chaiken, I. M. *Proc. Natl. Acad. Sci. U.S.A.* **1985**, *82*, 6423−6426.
(19) Martin, P. D.; Doscher, M. S.; Edwards, B. F. P. *J. Biol. Chem.* **1987**, *262*, 15930−15938.
(20) Varadarajan, R.; Richards, F. M. *Biochemistry* **1992**, *31*, 12315−12327.
(21) Usher, D. A.; Erenrich, E. S.; Eckstein, F. *Proc. Natl. Acad. Sci. U.S.A.* **1972**, *69*, 115−118.
(22) Usher, D. A.; Richardson, D. I.; Eckstein, F. *Nature* **1970**, *228*, 663−665.
(23) Hirs, C. H. W.; Halmann, M.; Kycia, J. H. *Arch. Biochem. Biophys.* **1965**, *111*, 209−222.
(24) Stern, M. S.; Doscher, M. S. *FEBS Lett.* **1984**, *171*, 253−256.
(25) Messmore, J. M.; Fuchs, D. N.; Raines, R. T. *J. Am. Chem. Soc.* **1995**, *117*, 8057−8060.
(26) Haydock, K.; Lim, C.; Brunger, A. T.; Karplus, M. *J. Am. Chem. Soc.* **1990**, *112*, 3826−3831.
(27) Lindquist, R. N.; Lynn, J. L.; Lienhard, G. E. *J. Am. Chem. Soc.* **1973**, *95*, 8762−8768.

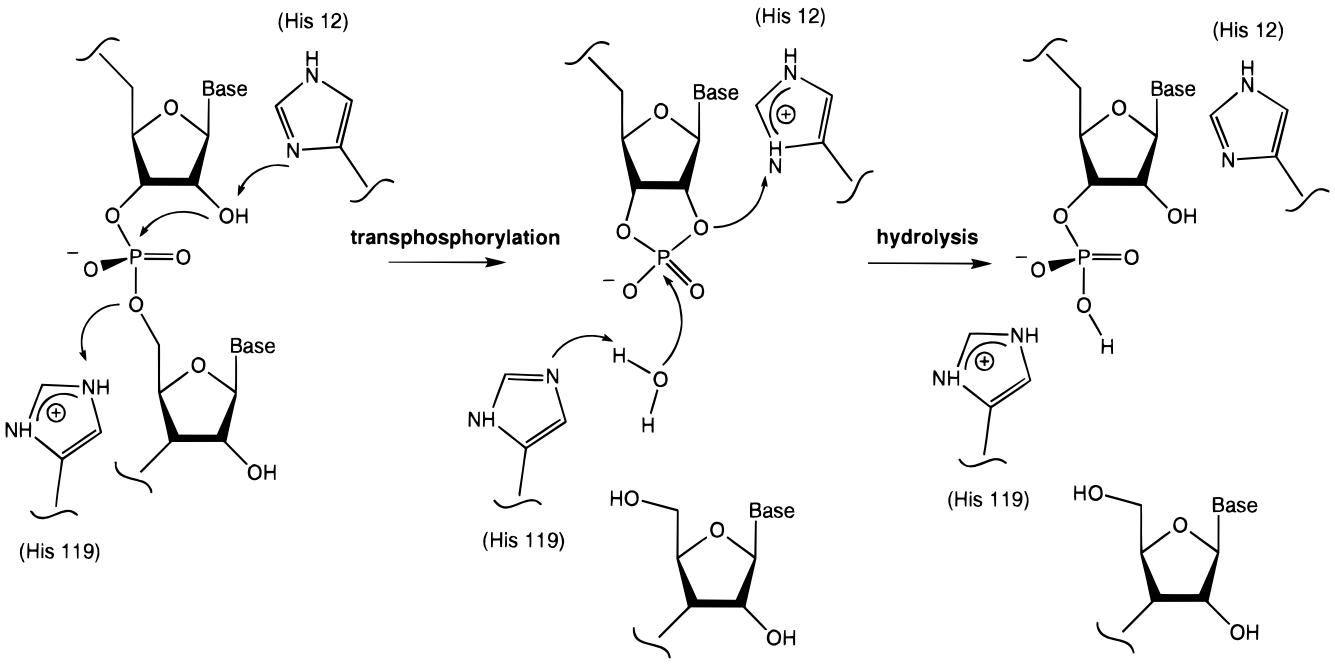


**Figure 2.** The generally accepted two-step catalytic reaction mechanism of bovine pancreatic RNase A.

achieve a pentacoordinate arrangement, might be useful as a stable analogue for the TBP phosphorane structures. Consistent with expectations, various vanadate species were found to be potent inhibitors for a series of enzymes involving phosphate ester hydrolysis or phosphoryl transfer including ATPases, phosphatases, and nucleases (see Crans et al. and references therein).[28] Despite the extensive solution-phase studies by Crans and others, only a few vanadate−enzyme complexes have been studied crystallographically and include a uridine vanadate RNase A complex,[29−31] *Aspergillus orzae* ribonuclease $T_1$-$H_2$-$VO_4^-$,[32] and rat acid phosphatase.[33] Surprisingly, a pentacoordinate oxy-vanadate has been observed crystallographically in the structures of only two of these systems, bovine RNase A and rat acid phosphatase. In the latter case, the vanadate is observed within coordination distance of His12 in the active site and therefore may not be a true pentacoordinate species.

Two different crystal structures of UV−RNase A complex have previously been reported,[29−31] and one of these has been compared with the results of high-field NMR studies of the complex.[31] The primary result of the first X-ray crystal structure analysis[29] was the determination of how a "transition state" like analogue influences the mobility of the important interacting active site residues. It was concluded that Lys41, in particular, becomes immobilized in the presence of UV and that the side chain of Lys41 interacts directly with one of the vanadate oxygens. The second structure of the UV−RNase A complex, determined using combined 2.0 Å X-ray and 2.2 Å neutron data,[30] and its comparison with the NMR results revealed several important features of the active site.[31] Similar to the earlier results, Lys41, His12, and His119 side chains were found to be in direct contact with UV; however, the interactions were inconsistent with expectations based on the previously proposed mechanism outlined in Figure 2. Specifically, His12 was found positioned to interact with an equatorial vanadate oxygen while the side chain of Lys41 was found closest to the axial O2′ oxygen. Recently, a UV−RNase A complex has been investigated using one- and two-dimensional NMR techniques.[34] On the basis of the appearance or absence of certain cross-peaks in the NMR spectrum, it was postulated that the position of the side chain of His119 may be different for the complex in solution than in the crystal structure. Although critical information has been determined from the structural studies of this most promising reaction intermediate or transition-state analogue thus far, much more work on UV−RNase A is required to extrapolate and better understand the actual RNase A enzymatic mechanism.

In the present study, the UV−RNase A complex is reinvestigated using refined X-ray data[35] collected at the highest resolution currently available for this bound enzyme (1.3 Å). In addition, ab initio quantum mechanical results on model oxy-vanadate compounds are used to help interpret the structural data and provide an initial starting guess for the crystallographic refinement process. One of the primary goals of the present work is to identify the most probable protonation state of the UV within the active site of RNase A. More specifically, to determine whether the UV exists as the mono- or dianion by a direct comparison of the high-resolution structure of UV−RNase A with those determined computationally. Finally, these results will be extended to determine what significance, if any, the protonation state may have on the true RNase A phosphate ester hydrolysis mechanism.

## Experimental and Computational Procedures

**Computational Details of the Mono- and Dianionic Vanadate Models.** The mono- and dianionic oxy-vanadate models used in this study as starting points in the X-ray refinement process are the pentacoordinate cyclic ethylene oxy-vanadates compounds ($EOV^-$ and $EOV^{2-}$), shown in Figures 3 and 4, respectively. Several different

(28) Crans, D. C.; Willging, E. M.; Butler, S. R. *J. Am. Chem. Soc.* **1990**, *112*, 427−432.
(29) Alber, T.; Gilbert, W. A.; Ponzi, D. R.; Petsko, G. A. *Ciba. Found. Symp.* **1983**, *93*, 4−24.
(30) Wlodawer, A.; Miller, M.; Sjolin, L. *Proc. Natl. Acad. Sci. U.S.A.* **1983**, *80*, 3628−3631.
(31) Borah, B.; Chen, C.; Egan, W.; Miller, M.; Wlodawer, A.; Cohen, J. S. *Biochemistry* **1985**, *24*, 2058−2067.
(32) Kostrewa, D.; Choe, W.-W.; Heinemann, U.; Saenger, W. *Biochemistry* **1989**, *28*, 7592−7600.
(33) Lindqvist, Y.; Schneider, G.; Vihko, P. *Eur. J. Biochem.* **1994**, *221*, 139−142.
(34) Veenstra, T. D.; Lee, L. *Biophys. J.* **1994**, *67*, 331−335.
(35) Ladner, J. E.; Wladkowski, B. D.; Svensson, L. A.; Sjölin L.; Gilliland, G. L. *Acta Crystallogr. D* **1997**, *D53*, 290−301.

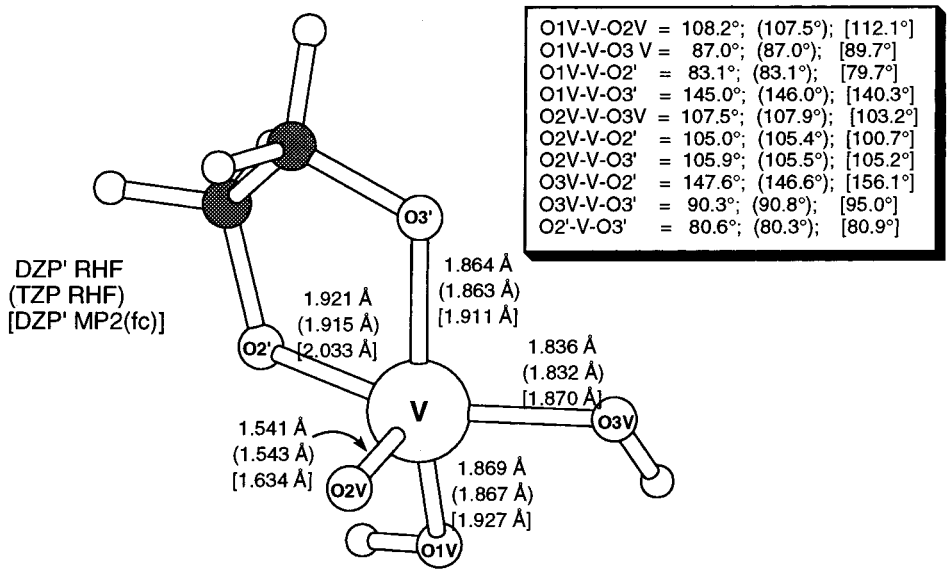


**Figure 3.** Monoanionic ethylene oxy-vanadate compound ($EOV^-$). Geometric parameters determined at three different ab initio quantum levels are indicated: (a) DZP′ RHF and (b) TZP RHF in parentheses and (c) DZP′ MP2 in brackets.

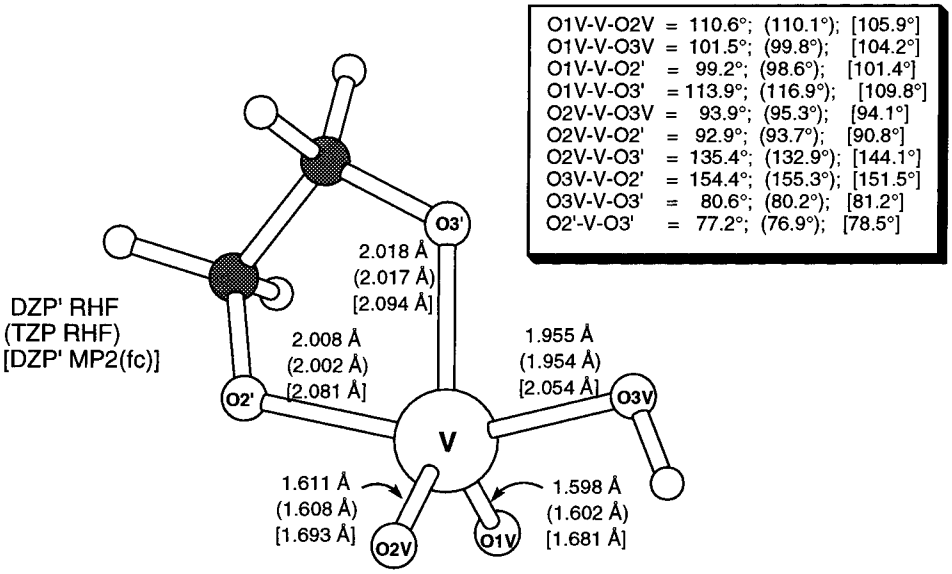


**Figure 4.** Dianionic ethylene oxy-vanadate compound ($EOV^{2-}$). Geometric parameters determined at three different ab initio quantum levels are indicated: (a) DZP′ RHF and (b) TZP RHF in parentheses and (c) DZP′ MP2 in brackets.

atomic orbital basis sets were used to determine the gas-phase structures, including a split-valence set in which the vanadium core orbitals are represented by the effective core potential (ECP) designated SBK-31G,[36] the valence double-ζ (DZ) set of Dunning[37] with a full triple-ζ basis for vanadium (DZ′), and finally a full triple-ζ basis on all atoms with contractions of (10s,6p)/[5s,3p] for C and O, (5s)/[3s] for H, and (14s,-11p,6d)/[10s,8p,3d] for V (TZ).[38] In the case of the smaller DZ′ basis set, a diffuse sp function [C($\alpha_{sp}$ = 0.0438), O($\alpha_{sp}$ = 0.0845)] and a single polarization function [C($\alpha_d$ = 0.750), O($\alpha_d$ = 0.850)] was appended to each C and O (DZP+R) to test their effects on the structures. In the case of the larger TZ basis set, a single polarization function was appended to C, O and V (TZP) and a single f-function was added to the vanadium [O($\alpha_d$ = 0.40)] (TZP+f) to probe the effects of these functions. The largest TZP+f basis sets consist of 220 and 217 contracted Gaussian functions, respectively, for $EOV^-$ ($C_2H_5O_5V^-$) and $EOV^{2-}$ ($C_2H_6O_5V^{2-}$), respectively. The electronic wave functions were determined by the single-reference, self-consistent-field, restricted Hartree−Fock (RHF) method.[39] Dynamical electron correlation effects were accounted for using second-order Møller−Plesset (MP2) perturbation theory.[39] The core orbitals were excluded from the active space in all correlated calculations. RHF and MP2 analytic gradient techniques were used to determine the optimized structures to $10^{-3}$ Å or rad in the internal coordinate space. All calculations were performed using the GAUSSIAN 92 electronic structure package.[40]

**Crystallographic Methods.** RNase A crystals used in the X-ray diffraction experiments were grown by implementing previously described procedures.[8] Crystals were grown at room temperature from solutions containing 100 mg/mL RNase A and 43% 2-methyl-2-propanol at pH 5.3. The UV solution was prepared by mixing 45 mg of uridine and 105 mg of $NH_4VO_3$ in 6.1 mL of 50 mM imidazole buffer followed by heating. New synthetic mother liquor was prepared

(36) Stevens, W. J.; Basch, H.; Krauss, M. *J. Chem. Phys.* **1984**, *81*, 6026−6033.

(37) Dunning, T. H.; Hay, P. J. In *Modern Theoretical Chemistry*; Plenum Press: New York, 1976.

(38) Wachters, A. J. H. *J. Chem. Phys.* **1970**, *52*, 1033−1036.

(39) Hehre, W. J.; Radom, L.; Schleyer, P. V. R.; Pople, J. A. In *Ab Initio Molecular Orbital Theory*; Wiley-Interscience: New York, 1986.

(40) *Gaussian 92*, Revision A; Fisch, M. J.; Trucks, G. W.; Head-Gordon, M.; Gill, P. M. W.; Wong, M. W.; Foresman, J. B.; Johnson, B. G.; Schlegel, H. B.; Robb, M. A.; Replogle, E. S.; Gomperts, R.; Andres, J. L.; Raghavachari, K.; Binkley, J. S.; Gonzalez, C.; Martin, R. L.; Fox, D. J.; Defrees, D. J.; Baker, J.; Stewart, J. J. P.; Pople, J. A.; Gaussian, Inc.: Pittsburgh, PA, 1992.

by the addition of 2-methyl-2-propanol to the UV solution to obtain a solution that contained 50% (v:v) alcohol. The final pH of the solution was 6.2. The crystal used for data collection was soaked for 10 days. Diffraction data were collected using a Siemens electronic area detector and processed with the XENGEN program system.[41] The X-ray structure of UV−RNase A was solved by a straightforward analysis of difference Fourier maps followed by least-squares refinement. The initial phases were estimated using the coordinates from the 1.26 Å phosphate-free structure of RNase A.[12]

The least-squares refinement of the X-ray structure was accomplished using the programs PROLSQ[42] and PROFFT.[43,44] Initially, a standard group for the UV was constructed using SYBYL and information from theoretical calculations.[45] After an initial adjustment of the model and inclusion of hydrogen atoms, typically 15 cycles of least-squares refinement were done before the model was examined and/or adjusted using the computer graphics program FRODO[46] and O.[47] A series of six refinement and rebuilding cycles was required to produce a three-dimensional structure that minimized the significant peaks in the $F_o - F_c$ difference Fourier maps.

The refinement was continued to help answer the more quantitative question relating to the protonation state of the UV in the active site of RNase A. Two independent refinements were initiated using either a monoanionic or a dianionic standard group on the basis of the structures calculated at the TZP RHF level of theory shown in Figures 3 and 4. These refinements were carried out in parallel using identical protocols with PROFFT. After 30 cycles of refinement, the resulting UV structures retained significant differences, particularly in the V−O bond distances. Before continuing, the refined UV coordinates of each structure were used to produce a new standard group for the restraints dictionary. An additional 6 cycles of refinement were performed using the updated restraints. Three iterations of this procedure were required before the resulting structures approached convergence. Two additional refinements were carried out using the mono- and dianionic starting models with all V−O bond restraints removed from the restraints dictionary. Thirty refinement cycles were carried out to reach convergence. The resulting coordinates of the UV groups from these four studies were indentical to within the limits of refinement error. The complete details of the refinement protocols and intermediate results have been presented elsewhere.[35]

The positions for all residues modeled with alternate conformations were verified by omit maps. Side chains of the residues with alternate conformations were removed, and five cycles of refinement were carried out before recalculating the electron density map. The final coordinates have been deposited in the Brookhaven Protein Data Bank[48] with the identifier 1RUV.

**Structure Comparisons.** The comparison analysis of UV−RNase A with other RNase structures required a computational optimization of the superpositioning of the protein molecules due to slight difference in the unit cell parameters. The superpositioning of the molecules was done with the ALIGN program[49] using only the $C_\alpha$ atom positions of the polypeptide backbone during the superposition procedure.

## Results

**Model Mono- and Dianionic Oxy-vanadate Structures.** Because oxy-vanadates undergo rapid polymerization in concentrated solutions, the crystallographic determination of the structure of these ion is difficult or impossible. Therefore, determination of the structure of oxy-vanadate species using computational methods plays a critical role in both the analysis and interpretation of the experimental data given. Krauss and Basch[45] were the first to use computational methods to study pentacoordinate oxy-vanadates as possible analogues for the phosphorane structure important in enzyme-catalyzed phosphate ester hydrolysis reactions. Initial work focused on the prototype TBP oxy-vanadate $H_4VO_5^-$ in comparison with the corresponding phosphorane analogue, $H_4PO_5^-$. Both the gas-phase structure and the electrostatic potential around the oxygens, determined at the RHF level using ECP basis sets, revealed interesting dissimilarity between the two systems. The geometry and electronic character of the anionic V−O and P−O bonds, in particular, were found to be distinctly different. As a result, it was argued that the TBP oxy-vanadate of UV−RNase A could not be used to analyze the real enzymatic mechanism involving phosphate ester hydrolysis. Krauss and Basch did point out, however, that proton transfer curves involving the prototype TBP oxy-vanadates or oxy-phosphoranes and compounds used to mimic amino acid residues found in the RNase A active site were essentially equivalent and that electronic differences between the two systems may not be the dominant factor influencing the use of vanadates as appropriate phosphorane analogues.

In the present study, a more realistic cyclic oxy-vanadate model is used to represent the UV inhibitor in the UV−RNase A complex. Shown in Figures 3 and 4 are three-dimensional representations of the mono- and dianionic ethylene oxy-vanadate model compounds, $EOV^-$ and $EOV^{2-}$, respectively, along with the important gas-phase structural parameters determined at three different ab initio quantum mechanical levels. As can be seen from these two figures, both structures are highly distorted TBPs in which the O2′ and O3V oxygens occupy the approximate axial position, and O1V, O2V, and O3′ oxygens occupy approximate equatorial positions in each case. The distortion of the TBP arrangement is evident from the value of the O3V−V−O2′ angle which was found to be less than 180° in both structures [154° ($EOV^-$) and 148° ($EOV^{2-}$), respectively, at the DZP′ MP2 level]. As expected on the basis of the details of the ab initio theoretical methodology, several important structural shifts are observed as the basis set is expanded, and as electron correlation is accounted for via MP2, most noticeably, in the latter case. In both structures, a slight contraction of most V−O bonds is seen (ca. 0.01 Å) at the RHF level as the basis set is expanded form DZP′ to TZP. The structural effects of the additional diffuse function and f-function were found to be negligible, and therefore, are not included in the figures. Electron correlation contributions to the vanadate structures were found to be much more significant. In both the mono- and dianionic structures, the V−O bonds elongate substantially (ca. 0.05−0.1 Å) in going from the DZP′ RHF to DZP′ MP2(fc); however, these shifts are consistent with shifts found for other transition metal complexes.[39]

Although it is extremely difficult to asses the accuracy of the $EOV^-$ and $EOV^{2-}$ structures determined computationally given the paucity of experimental data on oxo-vanadium compounds, especially pentacoordinate species, these structures can be evaluated using a valence-bond-order (vbo) analysis, such as the empirical approach established by Brown and co-workers.[50−53] Such an analysis can provide insight into the

(41) Howard, A. J.; Gilliland, G. L.; Finzel, B. C.; Poulos, T. L.; Ohlendorf, D. H.; Salemme, F. R. *J. Appl. Crystallogr.* **1987**, *20*, 383−387.
(42) Hendrickson, W. A.; Konnert, J. H. In *Biomolecular Structure, Conformation, Function and Evolution*; Srinivasan, R., Ed.; Pergamon Press: Oxford, 1980; Vol. 1.
(43) Finzel, B. C. *J. Appl. Crystallogr.* **1987**, *20*, 53−55.
(44) Sheriff, S. *J. Appl. Crystallogr.* **1987**, *20*, 55−57.
(45) Krauss, M.; Basch, H. *J. Am. Chem. Soc.* **1992**, *114*, 3630−3634.
(46) Jones, T. A. *J. Appl. Crystallogr.* **1978**, *11*, 268−272.
(47) Jones, T. A.; Zou, J.-Y.; Cowan, S. W.; Kjeldgaard, M. *Acta Crystallogr.* **1991**, *A47*, 110−119.
(48) Bernstein, F. C.; Koetzle, T. F.; Williams, G. J. B.; Meyer, E. F., Jr.; Brice, M. D.; Rogers, J. R.; Kennard, O.; Shimanouchi, T.; Tasumi, M. *J. Mol. Biol.* **1977**, *112*, 535−542.
(49) Satow, Y.; Cohen, G. H.; Padlan, E. A.; Davies, D. R. *J. Mol. Biol.* **1986**, *190*, 593−604.
(50) Brown, I. D.; Shannon, R. D. *Acta Crystallogr.* **1973**, *A29*, 266.
(51) Brown, I. D. *Acta Crystallogr.* **1976**, *A32*, 24.

overall character of these structures and can be used to determine whether or not these structures reasonably represent true pentacoordinate species. Application of the vbo analysis to $EOV^-$ and $EOV^{2-}$ results in the following total bond orders for the five V−O bonds in each structure: $EOV^-$ 5.36 vu (RHF DZP′), 4.33 vu (MP2(fc) DZP′), and $EOV^{2-}$ 5.24 vu (RHF DZP′), 4.13 vu (MP2(fc) DZP′). Although no result is exactly 5 as would be expected for a vanadate complex with a vanadium in the +5 oxidation state, the results are reasonable given the comparisons being made and the fact that the model developed by Brown and co-workers was based on condensed phase structural data. It is interesting to note that the total bond order is slightly larger for the monoanionic $EOV^-$ structure, independent of level of theory.

As mentioned above, one of the primary goals of the present study is to predict the most likely protonation state of the oxy-vanadate found in the UV−RNase A complex by comparing the theoretically determined model oxy-vanadate structures with the UV structure from the final X-ray refinement of the UV−RNase A complex. As a result, the individual structural features of the model vanadates themselves are much less important than the relative differences between them. Comparison of the relative structural data in Figures 3 and 4 reveals striking dissimilarities between the mono- and dianionic oxy-vanadate models. Except for V−O1V, all of the V−O bond distances are longer in the dianion structure. The two axial V−O bond lengths are 0.05 and 0.15 Å longer in $EOV^{2-}$ than in $EOV^-$ at the DZP′ MP2 level. The equatorial V−O3′ bond length is nearly 0.2 Å longer in $EOV^{2-}$ at the same level of theory. As expected, V−O1V contracts as the proton is removed (ca. 0.24 Å). A number of important differences in the bond angles between the mono- and the dianionic oxy-vanadate structures are found as well, most noticeably, those associated with the O1V and O2V oxygens. The O1V−V−O2′ angle expands (ca. 20°) and the O1V−V− O3′ angle contracts (ca. 30°), while the O2V−V−O3′ angle expands (ca. 40°) in going from the mono- to dianionic structure.

The most powerful comparative probe for the two structures is the qualitative ordering of the equatorial V−O distances. The monoanion structure, $EOV^-$, has two long and one very short equatorial V−O distances; more specifically, V−O1V is much longer than V−O2V (ca. 0.3 Å) at all computational levels. The dianionic structure, $EOV^{2-}$, however, has one very long equatorial V−O distance, V−O3′, and two that are moderately short. Most important, the V− O1V and V−O2V bond lengths in $EOV^{2-}$ are nearly identical at all ab initio levels considered here. This qualitative pattern can be used as an indicator for the protonation state of the UV bound in the UV−RNase A complex studied crystallographically.

**The High-Resolution X-ray Crystal Structure of the UV−RNase A Complex.** The structure of the UV−RNase A complex presented here is based on interpretation of the electron density map accounting for all 124 amino acid residues in the protein, the bound UV inhibitor, 131 water molecules, and a single 2-methyl-2-propanol molecule, leading to a final crystallographic *R* factor of 0.197. A summary of the refinement statistics resulting from the current analysis is given in Table 1. To illustrate the quality of the current diffraction data, a three-dimensional representation of the 1.3 Å $2F_o - F_c$ electron density map of the RNase A active site region containing the UV is shown in Figure 5. Since the details of the refinement process are not the focus of the present study, only a brief description will be given here for clarity. A more complete description including a detailed analysis of the multiple conformation residues and comparison with other related X-ray structures can be found in a recent related article.[35]

**Table 1.** Statistics on Crystallographic Analysis

| | |
|---|---|
| **Diffraction Data** | |
| space group | $P2_1$ |
| cell parameters (*a*, *b*, *c* in Å, $\beta$ in deg) | 29.8, 38.2, 53.2, 106.1 |
| resolution (Å) | 1.25 |
| measured intensities | 94 196 |
| unique reflns | 25 327 |
| possible reflns | 30 307 |
| $R_{sym}$ | 0.05 |
| **Refinement** | |
| *R* factor | 0.197 |
| resolution limits (Å) | 10.0−1.25 |
| **Geometry rms Deviation** | |
| bond length (Å) | 0.027 |
| angle distance (Å) | 0.038 |
| planarity (Å) | 0.017 |
| ideal chirality (Å) | 0.168 |

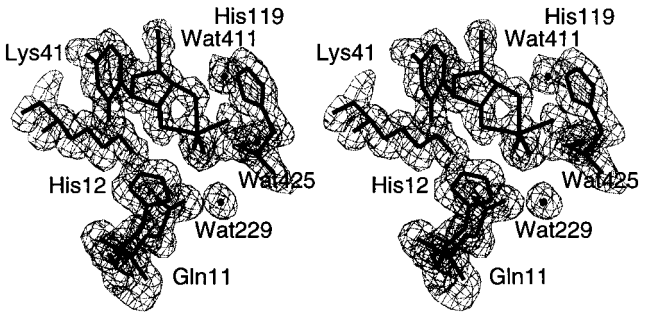


**Figure 5.** A representative sample of the final $2F_o - F_c$ electron density map of the RNase A−UV complex in the vicinity of the uridine binding site contoured at 1.0 Å.

Briefly, UV can be broken down into three regions including the TBP vanadate, the ribose ring, and the uridine base. These components interact with the RNase A active site at the $P_1$, $R_1$, and $B_1$ subsites, respectively. A three-dimensional representation of these subsites along with the UV is shown in Figure 6 illustrating the important hydrogen-bonding interactions (dashed lines) between each group. As seen in Figure 6, the $P_1$ subsite of RNase A is composed of atoms of the amino acid residues Gln11, His12, His119, Lys41, and Phe120 and water molecules Wat229, Wat411, and Wat425. The UV apical vanadate oxygens, O2′ and O3V, form interactions with a number of different $P_1$ components. Specifically, O2′ is within hydrogen-bond distance to Lys41 $N^{\zeta}$ (2.7 Å) and His12 $N^{\epsilon 2}$ to a lesser extent (3.4 Å), while O3V interacts primarily with His119 $N^{\delta 1}$ (2.6 Å), Wat425 (2.2 Å), and Wat411 (2.7 Å). The primary interaction between equatorial vanadate oxygens and components in the $P_1$ subsite include O3′, which is within hydrogen-bonding distance to Wat411 (2.6 Å) and to a lesser extent to His119 $N^{\delta 1}$ (3.2 Å), O1V that interacts with His12 $N^{\epsilon 2}$ (2.7 Å), Phe120 N (2.9 Å), and Wat229 (2.7 Å), and finally O2V is within hydrogen-bonding distance to Gln11 $N^{\epsilon 2}$ (2.9 Å). Although Lys7 has been postulated as a key active site residue in catalysis, it is not part of the $P_1$ subsite and is not directly involved in binding of the UV.

The $R_1$ ribose binding subsite (the ribose is defined as the five sugar ring atoms and C5′) includes residues His12, Lys41, Val43, His119, and Phe120 and water molecules Wat358, Wat411, and Wat414. The only significant interactions in the $R_1$ subsite, however, are those associated with Val43 and

(52) Brown, I. D.; Wu, K. K. *Acta Crystallogr.* **1976**, *B32*, 1957.
(53) Brown, I. D. *Acta Crystallogr.* **1992**, *B48*, 553−572.

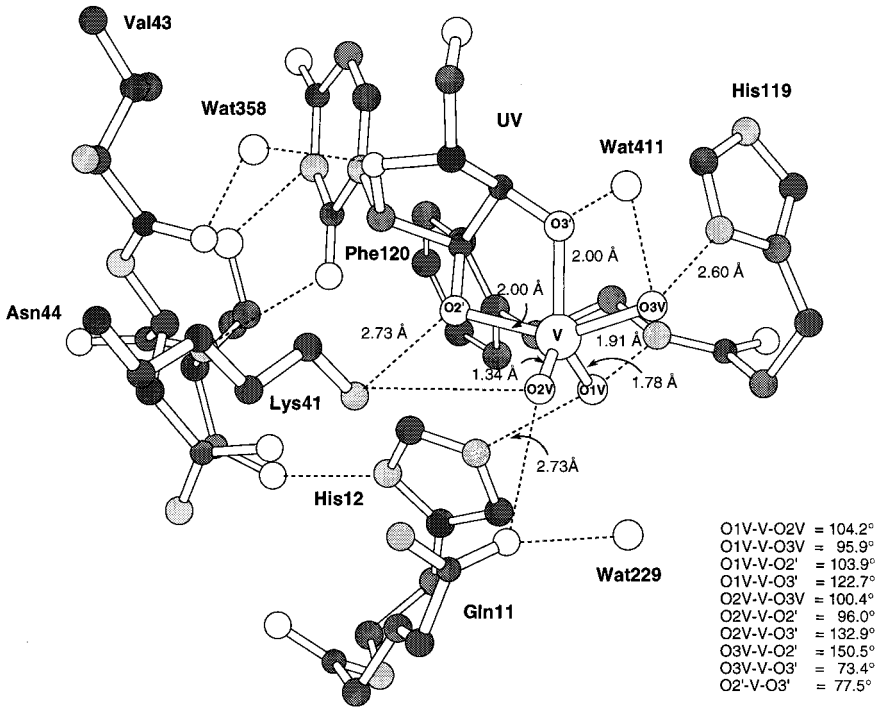


**Figure 6.** The UV in the active site of 1RUV with the associated basic residues His12, Lys41, and His119. The geometry including bond angles and distances of the TBP is shown.

Wat358. The ribose ring oxygen O4′ hydrogen bonds to Val43 O (3.4 Å). Wat358 is within hydrogen-bonding distance to a number of the $R_1$ components including Wat414 (3.1 Å), Val43 backbone (3.0 Å to O and 3.2 Å to N), the ribose oxygen O4′ (3.1 Å) as well as Wat365 (2.8 Å) found outside the $R_1$ subsite. From its many close contacts, Wat358 is clearly an essential structural component in this region.

The $B_1$ pyrimidine binding subsite formed by the six amino acid residues His12, Val43, Asn44, Asn45, Arg83, and Phe120 and two water molecules Wat310 and Wat373 has been described in detail recently by Gilliland and co-workers.[54] As seen in Figure 6, two important hydrogen bond interactions exists directly between protein atoms and the base. The peptide N of Thr45 is 2.9 Å from the uridine O2, while $O^{\gamma 1}$ of Thr45 is 2.7 Å from N3 of the uridine. The two conserved water molecules, Wat310 and Wat373, mediate the interaction of the nucleotide base with the protein and allow for the accommodation of any pyrimidine base in the $B_1$ pocket.

## Discussion

**Comparison of the Current UV−RNase A Structure with Other RNase A Complexes.** Over the years, several other RNase A structures with either a nucleotide or nucleotide analogue bound in the active site have also been determined. Comparison of the 1RUV with such complexes is useful to probe the applicability of oxy-vanadates as appropriate phosphorane analogues and to understand the necessary structural requirements to accommodate a pentacoordinate substrate versus a simple tetracoordinate substrate. Previous comparisons of RNase A structures have focused on general aspects of the active site or qualitative structural features of the entire protein;[12,17,55−57] however, in the present analysis, only the essential active site residues including those associated with the $B_1$, $R_1$, and $P_1$ subsites are of interest.

The current structure of the UV−RNase A complex, 1RUV, can be compared with five of the most recent (≤2.3 Å resolution) structures of the RNase A enzyme that contain various nucleotide and nonnucleotide analogues bound in the active site. These RNase A complexes, indicated here by their Brookhaven Protein Data Bank identifiers, include the following: 6RSA with bound UV,[9] 1ROB with bound 2′-cytidine-2′-phosphate,[58] 1RCN with bound d(ApTpApApG),[59] 1RPF with bound cytidine-3′-monophosphate,[17] and 1RPG with bound deoxycytidyl-3′,5′-deoxyadenosine.[17] In all of these complexes, the protein and solvent components that make up the $B_1$ subsite are very similar. The $B_1$ subsite can accommodate a uridine, cytidine, or thymidine and maintain the necessary hydrogen-bonding pattern.[54] The various structures, however, exhibit differences in the solvent interactions at the $B_1$ subsite. Both of the highly conserved water sites observed in 1RUV, Wat310 and Wat373, are found in all of the structures except 6RSA and 1RCN. The 2.0 Å resolution 6RSA structure contains only one water corresponding to Wat310, while the 2.3 Å resolution 1RCN structure does not contain any waters corresponding to Wat310 or Wat373. In both the 6RSA and 1RCN structures, the distances from N3, O2, and O4 of the base to the N and $O^{\gamma 1}$ of Thr45 are comparable to those found in the other complexes. The absence of these waters may be due to the lower resolution diffraction data used in the refinement.

Comparison of the $R_1$ subsite is obviously only relevant for those structures that include a substrate containing a ribose ring. These substrates include UV (1RUV and 6RSA), 2′-monophosphate (1ROB), 3′-monophosphate (1RPF), and deoxy-nucle-

(54) Gilliland, G. L.; Dill, J.; Pechik, I.; Svensson, L. A.; Sjolin, L. *Protein Pept. Lett.* **1994**, *1*, 60−65.
(55) Svensson, L. A.; Sjolin, L.; Gilliland, G. L.; Finzel, B. C.; Wlodawer, A. *Proteins, Struct. Funct. Genet.* **1986**, *1*, 370−375.
(56) Wlodawer, A.; Borkakoti, N.; Moss, D. S.; Howlin, B. *Acta Crystallogr.* **1986**, *B42*, 379−387.
(57) Crosio, M.-P.; Janin, J.; Jullien, M. *J. Mol. Biol.* **1992**, *228*, 243−251.
(58) Lisgarten, J. N.; Gupta, V.; Maes, D.; Wyns, L.; Zegers, I.; Palmer, R. A.; Dealwis, C. G.; Aguilar, C. F.; Hemmings, A. M. *Acta Crystallogr.* **1993**, *D49*, 541−547.
(59) Fontecilla-Camps, J. C.; de Llorens, R.; le Du, M. H.; Cuchillo, C. M. *J. Biol. Chem.* **1994**, *269*, 21526−21531.

otides (1RCN and 1RPG). In all cases, the ribose adopts a conformation that positions the base in the $B_1$ subsite and the phosphate or vanadate in the $P_1$ subsite. The reported 3′-*endo*-ribose conformations of 6RSA and 1ROB agree with that observed for 1RUV, but two other conformations of the ribose, 2′−*endo* (1RCN) and 2′−*exo* (1RPG and 1RPF), are also observed.

Because UV is the only pentacoordinate ligand of those listed above, all others being tetracoordinate, it is difficult to meaningfully compare features in the $P_1$ subsite. Moreover, because of the RNase A activity toward natural 3′−5′-dinucleotides, the bound tetracoordinate ligands in these complexes by necessity must be nonnatural structural variants and may include deoxyribose compounds, monophosphates such as 3′-CMP or 2′-5′−dinucleotides. As a result, when the backbone $C_\alpha$ atoms of 1RUV and the other structures are superimposed, the position of the phosphorus in the nucleotide-containing structures varies considerably from that of the vanadium by 0.1 Å for 1ROB, 0.5 Å for 1RCN, 0.6 Å for 1RPG, and 1.1 Å for 1RPF. Difficulty in comparison of the $P_1$ subsite of 1RUV with other RNase A complexes is illustrated further through a comparison with 1RPF, RNase A that contains 3′-CMP, a possible product from the actual enzymatic reaction. As in 1RUV, the O2′ oxygen of the 3′-CMP in 1RPF is within hydrogen bonding distance to both Lys41 $N^\zeta$ and His12 $N^{\epsilon 2}$, at 2.7 and 2.9 Å, respectively. However, when the $C^\alpha$ positions of the protein in both structures are superimposed, the remaining ligand oxygens are displaced significantly. In fact, O2P in 1RPF is closest to the position of O1V in 1RUV and is within similar bonding distance to His12 $N^{\epsilon 2}$ (2.7 Å) and Wat157 (2.7 Å) (that corresponds to Wat229 in 1RUV) in the $P_1$ subsite. If the nucleotide bases are superimposed, the 3′-CMP phosphorus in 1RFP is 1.6 Å from the position of the vanadium in 1RUV. Interestingly, the phosphorus and vanadium can be superimposed by a rotation about the C2′−C3′−O3′−P torsion angle of −66°. A similar shift in the position of the phosphorus relative to vanadium is reported by Alber and co-workers[29] in a previous cryocrystallographic study of RNase A. These results may suggest that a component of the actual enzymatic mechanism may involve rotation of the phosphate moiety to better accommodate the additional oxygen as the TBP oxy-phosphorane structure is being formed and rotation back to the original orientation once the product complex is produced.

Another feature of the active site that has shown some variation in the RNase A complexes studied crystallographically is the orientation of the His119 side chain. His119, a residue associated with both the $R_1$ and $P_1$ subsites, has been observed in two distinct conformations designated **A** and **B**.[60] The **A** conformation found in 1RUV has torsion angles of 149° for $\chi_1$ and −101° for $\chi_2$. This conformation is also reported in 6RSA, 7RSA, 1ROB, 1RCN, and 1RPG. Conformation **B** with torsion angle values near −69° for $\chi_1$ and near −63° for $\chi_2$ was originally reported as a minor component in unligated RNase A.[60] Interestingly, conformer **B** is the conformer reported for 1RPF. His119 conformer **B** is also present in the complex with O(3)-2′-CMP,[61] in a His12-alkylated derivative of RNase A[62] and postulated in NMR solution studies of unligated RNase A[63] and UV-ligated RNase A.[34] Both the **A** and **B** conformations are found in the 3RN3 and 1RPH structures. The conformational flexibility of His119 may also play a role in the actual enzymatic mechanism. In the **A** conformation, $N^{\delta 1}$ of His119 is in an ideal hydrogen-bonding position for a TBP structure in the active site, perhaps to aid in stabilization or to transfer a proton to the leaving group. Conversely, in the **B** conformation, the histidine ring is rotated out of the way, perhaps to allow the substrate to bind or the product to leave the active site.

**Trigonal Bipyramid Oxy-vanadate Structure.** Previous crystallographic structure analyses of the UV−RNase A complex focused primarily on details of the protein and the interaction of the active site residues with the UV inhibitor. Little attention was paid to the structural features of the UV itself. Quantifying the basic structural features of the bound UV inhibitor in the UV−RNase A complex is, however, an essential first step in answering questions regarding the applicability of oxy-vanadates as true phosphorane analogues and the implication of the UV structure on the actual RNase A enzymatic mechanism. Fortunately, the systematic refinement of the structure at high resolution (1.3 Å) described above, allows quantitative estimates of the basic structural feature of the bound inhibitor to be made for the first time.

As seen in Figure 6, the pentacoordinate vanadate structure is a distorted TBP with the O2′ and O3V oxygens occupying the apical positions and the O1V, O2V and O3′ oxygens occupying approximate equatorial positions around the vanadium. The distortion of the TBP arrangement is evident from the O−V−O angles also included in Figure 6. Several angles, including O3V−V−O2′ and O3V−V−O3′ deviate significantly from those expected for a true TBP (with deviations of 29.5° and 18°, respectively). However, the most important diagnostic structural features of the vanadate are the V−O distances themselves. Also shown in Figure 6, the crystallographically determined V−O distances vary considerably and are only qualitatively consistent with typical TBP's in which the axial bond distances are elongated relative to those in the equatorial plane.[28] It is interesting to note that although the two axial V−O distances are similar (1.91 and 2.00 Å), the equatorial V−O distances are extremely asymmetric ranging from 1.34 Å for V−O2V to 2.0 Å for V−O3′. These significant distortions of the TBP suggest that the bonding interactions involving the oxygens surrounding the vanadium are atypical or are influenced by factors other than those expected for a typical TBP transition-metal complex. The latter may be more appropriate given the direct influence of the active site environment on the vanadate structure, as evident from the data in Figure 6. Each of the vanadate oxygens interacts primarily with only one protein component in the RNase A active site. O1V interacts with $N^{\epsilon 1}$ of His12, O2V interacts with $N^{\epsilon 2}$ of Gln11, O3V interacts with $N^{\delta 1}$ of His119, O2′ interacts with $N^\zeta$ of Lys41, and O3′ interacts primarily with $N^{\delta 1}$ of His119. Distortion of the TBP oxy-vanadate framework is consistent with these important interactions, disrupting the TBP arrangement to optimize interactions with the active site. This is most noticeable for O3V that is displaced out of the apical plane and toward $N^{\delta 1}$ of His119, to achieve the short 2.6 Å interatomic distance. Without these distortions the five vanadate oxygens cannot form close contacts with the protein atoms. Apparently, the electronic structure of the TBP oxy-vanadate is such that significant distortion of the TBP framework is possible to allow for necessary interactions with the active site and may provide the explanation for the ability of UV to act as a strong inhibitor despite electronic differences with the corresponding phosphorane reported previously.[45]

(60) Borkakoti, N.; Moss, D. A.; Palmer, R. A. *Acta Crystallogr.* **1982**, *B38*, 2210−2217.

(61) Borkakoti, N.; Palmer, R. A.; Haneef, I.; Moss, D. S. *J. Mol. Biol.* **1983**, *169*, 743−755.

(62) Nachman, J.; Miller, M.; Gilliland, G. L.; Carty, R.; Pincus, M.; Wlodawer, A. *Biochemistry* **1990**, *29*, 928−937.

(63) Rico, M.; Santoro, J.; Gonzalez, C.; Bruix, M.; Neira, J. L.; Nieto, J. L.; Herranz, J. *J. Biomol. NMR* **1991**, *1*, 283−298.

One of the most important unresolved questions about the UV−RNase A complex is the protonation state of the UV in the RNase A active site. The protonation state at various stages along the reaction pathway for the actual RNase A enzymatic mechanism, including the proposed TBP phosphorane structure, has been an issue of considerable debate for many years. It has been argued that stabilization of key intermediates or transition states is made possible primarily through proton transfer to the developing anionic phosphorane. To the extent that the electrostatics of the UV mimics those of the true TBP phosphorane structure, the protonation state of the UV should provide insight into the nature of the corresponding phosphorane. Although protons cannot be observed directly in the electron density map obtained from the X-ray diffraction data, their presence (or absence) can be inferred, in certain cases, from the relative positions of the heavy atoms. *If the electronic and geometric structure of the system is strongly influenced by the overall protonation state, geometric patterns can be used to predict the most probable protonation state of the bound substrate.*

Comparison of the basic structural features (V−O bond distances and O−V−O angles) of the TBP oxy-vanadate portion of the UV from the final X-ray refinement shown in Figure 6 with the same features from the model oxy-vanadates determined computationally ($EOV^-$ and $EOV^{2-}$) shown in Figures 3 and 4 clearly shows the final X-ray structure is more similar to the model monoanionic structure, $EOV^-$, than with the model dianionic structure, $EOV^{2-}$. Although the relative ordering of all V−O bond distances around the TBP vanadium are not in complete agreement, the overall V−O bond distance pattern is similar. In particular, the bond distances associated with the nonbridging equatorial oxygens (V−O1V and V−O2V) were found to be highly asymmetric in the final X-ray refined structure, consistent with that found for the $EOV^-$ and not $EOV^{2-}$. Given the dramatic effect of protonation of the electronic character of the oxy-vanadates and its influence on the final structure, these data strongly suggest that in the bound UV−RNase A complex the O1V oxygen is protonated and the O2V oxygen is not, resulting in an overall monoanionic UV inhibitor.

Although the comparative data is suggestive that the UV in the RNase A active site is monoanionic, there are a number of unexplained structural differences in the final X-ray refined 1RUV structure and the monoanionic computational model, $EVO^-$. The most noticeable of these differences is that the V−O distances themselves that differ by as much as 0.2 Å. Specifically, the equatorial V−O2V distance in the final X-ray refined structure is exceedingly short (1.34 Å): over 0.2 Å shorter than the shortest V−O distance in $EOV^-$ at any quantum mechanical level. Moreover, if the valence bond order analysis developed by Brown and co-workers[50−53] is applied to the UV structure in 1RUV determined crystallographically and shown in Figure 6, a total valence bond order of 7.5 vu is obtained. This exeedingly high value is a direct results of the short V−O2V bond which contributes over 4 vu to the total. The remaining V−O distances were all longer in the X-ray structure compared to those determined computationally for $EOV^-$ by 0.1 Å or less. A number of differences in the O−V−O angles ranging from as little as 3° to as much as 27° for O2V−V−O3′ are also observed.

Many of the observed discrepancies between the experimental and theoretical UV structural features mentioned above can be accounted for from uncertainties in the respective data. Absolute errors in both the computational and experimental structural results as high as 0.1 Å in the bond distances and 10° in the bond angles are not unexpected given the known approximation in the computational methodology and given the resolution of the X-ray data. The discrepancy in the V−O2V distance between that found computationally and the value obtained from the crystallographic refinement (0.2−0.4 Å depend on the level of theory), however, is unlikely to be the result of systematic error. Moreover, the exceedingly short V−O2V bond distance found crystallographically is also inconsistent with the V−O distances obtained from the crystal structures of small model pentacoordinate oxy-vanadate compounds[64,65] and the vbo formalism of Brown and co-workers.[50−53] Several possible reasons for this discrepancy may be considered. First, experimental or computational factors may have influenced the refinement and the interpretation of the vanadate structure. This seems unlikely because of the care taken to ensure convergence of the crystallographic refinement. There is also the possibility the UV−RNase A crystals from which the X-ray data was collected contained a mixture of vanadate species, each contributing to the total density map. Some of the these species might include a vanadate in a different oxidation state, or dimeric/polymeric vanadates. Although the explanations based on a contaminated sample may be used to rationalize the unusually short V−O bond distance, there is no experimental evidence to support them. Perhaps a more probable explanation for the unusually short V−O2V bond is that the protein electrostatic environment is introducing significant perturbations in the electronic structure of the vanadate. One might conceptualize this as the enzyme influencing the structure of the vanadate to adopt a phosphorane-like structure or intermediate. Further experimental and computational work to probe this latter hypothesis is currently underway.

**Implications for the RNase A Catalytic Mechanism.** Although other mechanisms of varying complexity have been proposed over the years, the generally accepted catalytic mechanism, by which RNase A hydrolyses RNA strands, is the simple two-step general acid−base process shown schematically in Figure 2. As seen in the figure, both the transphosphorylation step and the subsequent hydrolysis step take place via inversion displacement at the phosphorus center, presumably through a TBP pentacoordinate phosphorane structure in which the His12 and His119 active site residues facilitate the proton transfer to and from the substrate. This mechanism has grown in popularity over the years because of its simplicity and because it appears consistent with most of the available structural, kinetic, and spectroscopic data; however, a number of controversies regarding specific details remain. Much of the controversy centers around the character of the proposed TBP phosphorane structure. Whether it is a true transition state or an intermediate, what is its protonation state, and to what extent certain active site residues intimately interact and stabilize the phosphorane structure are all issues of much debate.

In recent years, much of the work on the RNase A enzyme has focused on elucidating more detailed aspects of the microscopic mechanism in an attempt to understand how RNase A functions. Breslow[66] has summarized studies that show the microscopic mechanism by which RNase A functions to catalyze the hydrolysis of the phosphate ester to be more complicated than previously thought. Kinetic and temperature jump experiments using $\beta$-cyclodextrins as enzyme mimics have shown that

(64) Crans, D. C.; Felty, R. A.; Miller, M. M. *J. Am. Chem. Soc.* **1991**, *113*, 265−269.
(65) Angus-Dunne, S. J.; Batchelor, R. J.; Tracey, A. S.; Einstein, F. W. B. *J. Am. Chem. Soc.* **1995**, *117*, 5292−5296.
(66) Breslow, R. *Acc. Chem. Res.* **1991**, *24*, 317−324.

an initial catalytic proton transfer to neutralize the substrate occurs in conjunction with nucleophilic attack at the phosphorus. Moreover, Breslow has argued that it is His119 which acts to protonate the substrate in the initial step leading to an overall neutral phosphorane structure. On the basis of previously determined kinetic data from thio-substituted dinucleotide substrates, Herschlag[67] has argued against the mechanism proposed by Breslow or any other "triester-like" mechanism, suggesting that the thio effects results obtained were more consistent with the classical mechansim shown in Figure 2 where the active site residues do not formally undergo proton transfer with the substrate during transphosphorylation.

Various aspects of the RNase A mechanism have also been the subject of many computational studies over the years leading to a number of slightly different proposed microscopic mechanisms. Karplus and co-workers[26,68] have been involved in extensive molecular mechanics and dynamics simulations of the RNase A system and have shown among other things that certain key residues can undergo significant reorganization to fulfill catalytic functionality. Lim and Tole[69] have also proposed a detailed microscopic mechanism for RNase A catalyzed transphosphorylation based on ab initio quantum mechanical results of the a model substrate system in the gas phase. In their proposed mechanism, His12 acts to shuttle a proton from the O2′ oxygen to a phosphoryl oxygen on the substrate prior to nucleophilic attack of the O2′ oxygen on the phosphorus center. In doing so, an anionic nucleophile attacks a neutral phosphate ester. Lys41 in its protonated form maintains an initimate interaction with the O2′ oxygen on the substrate throughout the transphosphorylation process, but is shown not to formally transfer a proton to the substrate. In addition, Lim and Tole argue that His119, in its protonated form, acts to stabilize the substrate through interaction with another nonbridging phosphoryl oxygen in the initial stages of transphosphorylation and moves to donate a proton to O5′ in the final step. Finally, Wladkowski et al.[70,71] constructed a detailed model of the RNase A active site using ab initio quantum mechanical methods to probe features of the transphosphorylation reaction pathway. Among other things, it was discovered that the TBP phosphorane structure may be a true intermediate and exceedingly stable in the presence of the active site residues. Moreover, Lys41 was found to play an active role in the enzymatic mechanism, interacting directly with the phosphorane intermediate to undergo formal proton transfer.

The three-dimensional structure of the UV−RNase A complex presented here also provides valuable insight into the details of the actual RNase A enzymatic mechanism. Without participation of any other active site components the simplified mechanism described in the Introduction above (Figure 2) is consistent with formation of a dianionic intermediate phosphorane structure. Both steps of the mechanism involve a monoanionic nucleophilic attack on an monoanionic substrate. Analysis of the UV inhibitor structural data, however, suggests the TBP oxy-vanadate bound in the active site of the UV−RNase A complex is monoanionic. To the extent that the electrostatics of an oxy-vanadate mimic those of the corresponding oxyphosphorane one would expect the phosphorane structure important in the hydrolysis of polynucleotides to be monoanionic also. Moreover, the UV structural data described above are consistent with the O1V oxygen being the one protonated. From its proximity, His12 is the most likely source for this proton. Such an observation has interesting implication regarding the actual catalytic mechanism. If the proposed mechanism in which His12 acts as the catalytic general base-acid in the two steps of the overall mechanism is true, than His12 must also play an added, although perhaps secondary, role involved in stabilization of the phosphorane structure through proton transfer. Such a process has been proposed involving Lys41.

Perhaps the most striking features of the UV−RNase A active site region with direct implication to the RNase A mechanism is the position of the three important residues, His12, Lys41, and His119, relative to the UV inhibitor and to one another. As seen in Figure 6 and noted above, His12 is in a position to allow $N^{\epsilon 2}$ to interact directly with the nonbridging O1V oxygen, Lys41 $N^{\zeta}$ is closest to the O2′ oxygen, while His119 is positioned proximate to O3V. As pointed out by Wlodawer and coworkers[30] in their earlier work, the position of His12 and Lys41 appear reversed from that expected from the simplified mechanism described above. It would appear that Lys41 is optimally positioned to act as the catalytic base while His12 is optimally positioned to provide the stabilizing proton transfer to the anionic TBP intermediate. Although improbable given the relative solution phase p$K_a$ data of Lys41 and His12, this proposal was energetically feasible on the basis of the computational work of Wladkowski et al.[70,71]

Together, these data suggest several important aspects regarding the RNase A microscopic mechanism including the following: (1) Although p$K_a$ data from the unbound enzyme would suggest that the most likely general base for removal of the proton from the 2′-OH group on the ribose ring in the initial transphosphorylation step is His12, the structural results presented here, along with previous computational results imply that His12 is more appropriately positioned to interact with and neutralize the nonbridging phosphoryl oxygen. (2) To the extent that the electrostatics and resultant proton affinities of the bound uridine vanadate in UV−RNase A is similar to the true phosphorane structure appropriate to the enzymatic reaction pathway, the structural results presented here imply that such a TBP phosphorane structure is also likely to be monoanionic, with O1V being protonated. Moreover, given that monoanionic oxy-phosphoranes represent stable intermediates and not transition states, based on quantum mechanical results in the gas phase, the corresponding phosphorane applicable to the enzymatic reaction is also likely to be a true intermediate as opposed to a transition state. (3) Because of its close proximity, His12 is the only reasonable source of the proton which must end up on O1V. Such an observation strongly suggests that if His12 does act as the general base to remove the 2′-OH proton, it must also play a secondary role in neutralizing O1V as the TBP is formed. One could envision a process by which His12 shuttles the proton between O2′ and O1V in either a stepwise or concerted process. (4) Due to its close proximity to both the O2′ and the nonbridging O2V oxygen in the UV−RNase A complex, Lys41 is likely to play an intimate role in the enzymatic mechanism. In addition, if the dielectric constant of the enzyme active site is lowered enough when the substrate binds and key water molecules are displaced, Lys41 may be able to act as the general base in the first step, as it is optimally positioned to. (5) His119 is optimally positioned to protonate the leaving group in the initial transphosphorylation step but may rotate into position only after the substrate is bound. Collectively, these observation can be used to formulate the two

(67) Herschlag, D. *J. Am. Chem. Soc.* **1994**, *116*, 11631−11635.
(68) Staub, J. E.; Lim, C.; Karplus, M. *J. Am. Chem. Soc.* **1994**, *116*, 2591−2599.
(69) Lim, C.; Tole, P. *J. Am. Chem. Soc.* **1992**, *114*, 7245−7252.
(70) Wladkowski, B. D.; Krauss, M.; Stevens, W. J. *J. Phys. Chem.* **1995**, *99*, 6273−6276.
(71) Wladkowski, B. D.; Krauss, M.; Stevens, W. J. *J. Am. Chem. Soc.* **1995**, *117*, 10537−10545.

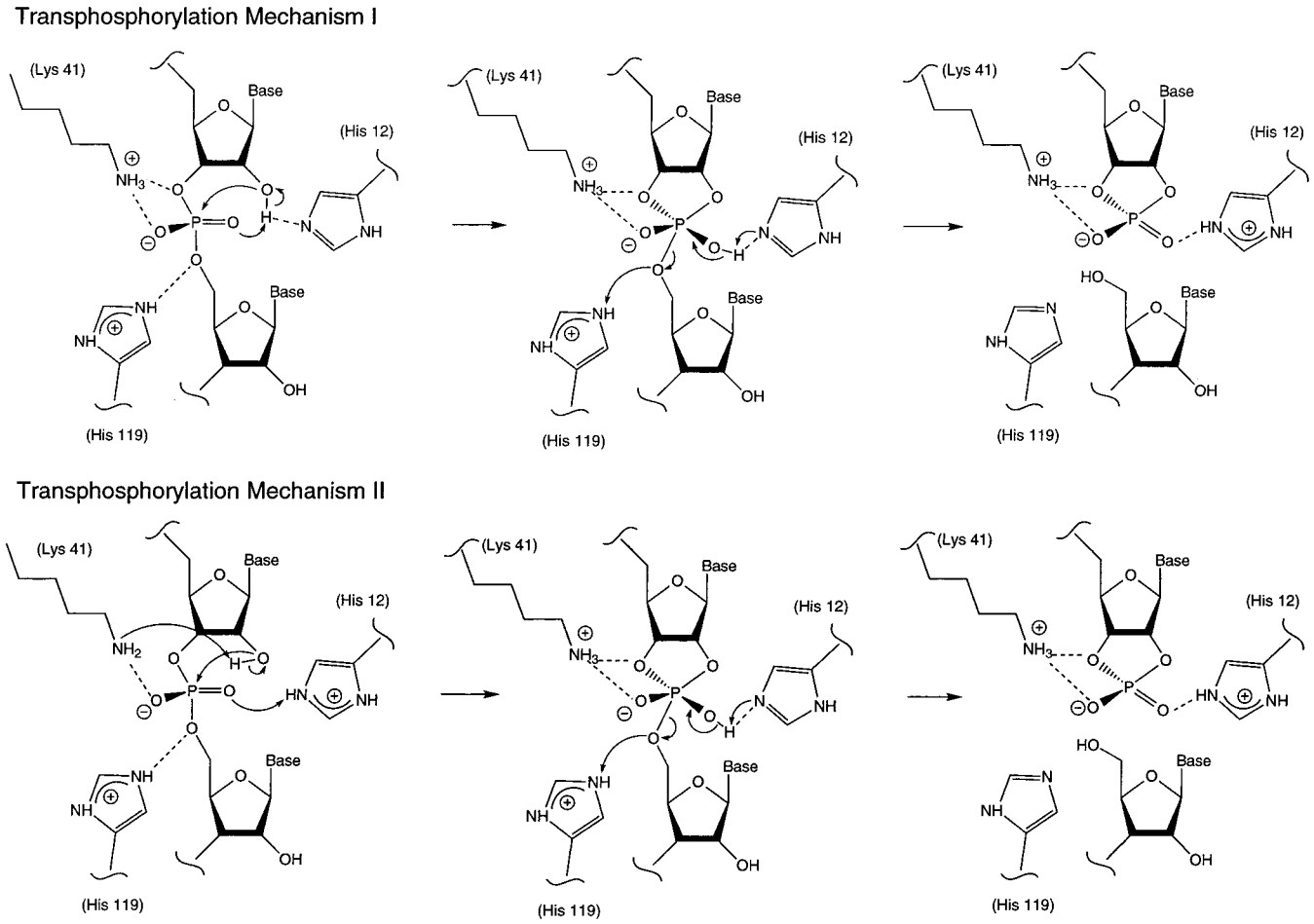


**Figure 7.** Proposed microscopic mechanisms (I and II) of RNase A based on the current UV−RNase A structure and previous computational results.

possible microscopic transphosphorylation mechanisms shown in Figure 7, where in mechanism I His12 acts as the proton shuttle, and in mechanism II, Lys41 acts as the catalytic base.

These two microscopic mechanism for RNase A transphosphorylation differ in several fundamental ways with the mechanisms previously propsed, both in the sequence of steps and the degree of involvement of key residues. Specifically, we believe Lys41 intimately participates in the reaction, either to act as the general base (Mechanism II) or to formally protonate the phosphorane intermediate (mechanism I), whereas previous mechanisms show Lys41 acting only to stabilize the phosphorane through electrostatic interactions. Moreover, due to the crystallographic position of His119 in the UV−RNase A complex, this residue is not oriented to formally protonate either of the nonbridging phosphoryl oxygen on the substrate, but instead is position perfectly to protonate the leaving group O5′ oxygen. It is important to recognize that many of the differences between the current mechanisms and those proposed previously are subtle, and considerable additional work, both experimental and computational, needs to be done in order to definitively resolve these issues.

**Acknowledgment.** The authors thank Morris Krauss, Walter Stevens, Sarah Chenoweth, and Kendra Jones for helpful discussions. We are also grateful to the referees for helpful comments and making us aware of the vbo formalism of Brown and co-workers. Certain commercial equipment, instruments, and materials are identified in this paper in order to specify the experimental procedure. Such identification neither implies recommendation or endorsement by the National Institute of Standards and Technology nor that the material or equipment identified are necessarily the best available for the purpose. We also thank Johnothan Dill for the use of unpublished algorithms and programs. Finally, B.D.W. is grateful to the Cottrell College Science Program and support through the Research Corporation.

JA972296N